

Adaptive linear second-order energy stable schemes for time-fractional Allen-Cahn equation with volume constraint

Bingquan Ji* Hong-lin Liao[†] Yuezhen Gong[‡] Luming Zhang[§]

Abstract

A time-fractional Allen-Cahn equation with volume constraint is first proposed by introducing a nonlocal time-dependent Lagrange multiplier. Adaptive linear second-order energy stable schemes are developed for the proposed model by combining invariant energy quadratization and scalar auxiliary variable approaches with the recent $L1^+$ formula. The new developed methods are proved to be volume-preserving and unconditionally energy stable on arbitrary nonuniform time meshes. The accelerated algorithm and adaptive time strategy are employed in numerical implement. Numerical results show that the proposed algorithms are computationally efficient in multi-scale simulations, and appropriate for accurately resolving the intrinsically initial singularity of solution and for efficiently capturing the fast dynamics away initial time.

Keywords: Time-fractional Allen-Cahn equation with volume constraint; invariant energy quadratization; scalar auxiliary variable; $L1^+$ formula; unconditional energy stable

AMS subject classifications. 35Q99, 65M06, 65M12, 74A50

1 Introduction

The gradient flow models are frequently used to describe relaxation dynamics that obey the second law of thermodynamics, ranging from materials science, fluid dynamics and engineering [1–3]. One of well-known models is the Allen-Cahn equation, which was originally introduced to model the anti-phase domain coarsening in a binary alloy [1]. Also, in the past decades, the Allen-Cahn equation and its various variants have been applied for a wide range of phenomena due to its advantages for microstructure numerical simulations, for instance, grain growth [4] and crystal growth [5]. However, considering the phase variable represents the volume fraction of material component, the classical Allen-Cahn equation does not conserve the initial volume.

*Department of Mathematics, Nanjing University of Aeronautics and Astronautics, 211101, P. R. China. Bingquan Ji (jibingquanm@163.com).

[†]Corresponding author. ORCID 0000-0003-0777-6832; Department of Mathematics, Nanjing University of Aeronautics and Astronautics, Nanjing 211106, P. R. China. Hong-lin Liao (liaohl@csrc.ac.cn and liaohl@nuaa.edu.cn) is supported by a grant 1008-56SYAH18037 from NUAA Scientific Research Starting Fund of Introduced Talent.

[‡]Department of Mathematics, Nanjing University of Aeronautics and Astronautics, Nanjing 210016, P. R. China; Yuezhen Gong (gongyuezhen@nuaa.edu.cn) is partially supported by the NSFC grant No. 11801269, and the NSF grant No. BK20180413 of Jiangsu Province.

[§]Department of Mathematics, Nanjing University of Aeronautics and Astronautics, 211101, P. R. China. Luming Zhang (zhanglm@nuaa.edu.cn) is supported by the NSFC grant No. 11571181.

To fix this drawback, the first work was given by Rubinstein and Sternberg, who added a time-dependent Lagrange multiplier to the original equation arising from an enforcement of conservation of volume [6]. Brassel and Bretin introduced another remedy to preserve the total volume-conservative property, i.e., they imposed local and nonlocal effects on the primitive model [7]. Recently, the time, space and time-space fractional Allen-Cahn equations were suggested to accurately describe anomalous diffusion problems [8–10]. However, they don't preserve the volume conservation. In this paper, we are going to develop a new time-fractional Allen-Cahn equation by enforcing a nonlocal Lagrange multiplier to cancel out the variation of volume, while without influencing the primitive energy dissipative property.

An alternative model for the gradient flow system is the Cahn-Hilliard equation, which naturally possesses the volume-preserving property [2]. The Allen-Cahn model with a volume constraint has been studied and compared with the Cahn-Hilliard model in [6]. The authors suggested that the Allen-Cahn model with a volume constraint is more appropriate for simulating the interfacial dynamics of immiscible multi-component material systems. And the order of Allen-Cahn equation is substantially lower than that of the Cahn-Hilliard equation, which implies that it may be relatively easier to simulate numerically. Some interesting insight may be offered by carrying out comparison investigations of volume conservative phased field models [11,12].

There have been a great amount of works to develop energy stable schemes for the gradient flow model. The early well-known numerical approaches include the convex-splitting technique and the stabilizing method. Readers are referred to [13,14] for more details. Recently, Yang et al. proposed a new numerical idea of recasting the free energy into a quadratic functional to design linear, second-order, unconditionally energy stable schemes, which called the invariant energy quadratization (IEQ) method [15]. Subsequently, Shen et al. developed the scalar auxiliary variable (SAV) approach, which was shown to be more effective than the IEQ approach [16]. In fact, the common goal of IEQ and SAV strategies is to first transform the original PDE system into a new equivalent system with a quadratic energy functional and the corresponding modified energy dissipation law. Specifically, applying the energy stable algorithms derived by the two energy quadratization strategies, the volume-preserving Allen-Cahn model was compared with the classical Allen-Cahn model as well as the Cahn-Hilliard model [17]. For more discussions and the applications of IEQ and SAV strategies, we refer to [15–18] and the references therein.

Along the numerical front with respect to the fractional phase field models, there are a lot of works devoted to the investigation on the solutions of the nonlocal models. Precisely, Hou et al. [8] showed that the space-fractional Allen-Cahn equation could be viewed a L^2 gradient flow for the fractional analogue version of Ginzburg-Landau free energy function. Meanwhile, the authors proved that the proposed numerical scheme preserves the energy decay property and the maximum principle in the discrete level. Li et al. [9] investigated a space-time fractional Allen-Cahn phase field model that describes the transport of the fluid mixture of two immiscible fluid phases. They concluded that the alternative model could provide more accurate description of anomalous diffusion processes and sharper interfaces than the classical model. The first theoretical contribution regarding the energy dissipation property of the time-fractional phase models was done by Tang et al. [19]. They proved that the time-fractional phase field models indeed admit an energy dissipation law of an integral type. In addition, they applied the uniform L1 formula to construct a class of finite difference schemes, which can preserve the theoretical energy dissipation property. Very recently, Du et al. [20] studied the time-fractional Allen-Cahn

equation, where the well-posedness, solution regularity, and maximum principle were proved rigorously. In addition, several unconditionally solvable and stable time-stepping schemes were developed. Also, the related convergence of those numerical approaches were established without any extra regularity assumption on the exact solution. Zhao et al. [10, 21] studied a series of the time-fractional phase field models numerically, including the time-fractional Cahn-Hilliard equation with different types of variable mobilities and time-fractional molecular beam epitaxy model. The considerable numerical evidences indicate that the effective free energy or roughness of the time-fractional phase field models during coarsening obeys a similar power scaling law as the integer ones, where the power is linearly proportional to the fractional index α . In other words, the main difference between the time-fractional phase field models and integer ones lies in the time-scales of coarsening.

In this paper, we first apply the IEQ/SAV approaches to reformulate the time-fractional phase field models into an equivalent system. Then the nonuniform $L1^+$ formula proposed in [22] is applied for the equivalent time-fractional model to develop linear, second-order energy stable numerical schemes, which are proved to preserve the volume conservation law and unconditionally energy stability on arbitrary nonuniform time meshes. Since the solution lacks the smoothness near the initial time although it would be smooth away from $t = 0$ [23, 24], the predicted second-order time accuracy of $L1^+$ formula is always restrictive. Actually, in any numerical methods for solving time-fractional diffusion equations, a basic consideration is the initial singularity of solution, see the recent works [25–27]. Based upon the realistic assumptions on the exact solution, we utilize the $L1^+$ formula on nonuniform time steps to compensate the intrinsically weak singularity of time-fractional models near initial time. We will show that the graded mesh can recover the optimal time accuracy when the solution is non-smooth near $t = 0$ numerically. In addition, in order to overcome the global dependence of historical solutions of time-fractional Caputo derivative, a fast variant of $L1^+$ formula is used to significantly reduce the computational complexity and the storage requirements. Since the evolution of time-fractional phase field models involves multiple time scales, adaptive time step strategy based on the evolution of total energy are reported to efficiently resolve widely varying time scales.

The outline of the article is arranged as follows. The time-fractional Allen-Cahn equation and its volume-conserving version as well as the time-fractional Cahn-Hilliard model are reported in Section 2. We then present the corresponding energy stable numerical schemes in Section 3. In Section 4, several numerical examples are performed to confirm the theoretical findings, covering the volume conservation and energy dissipation properties, and provide new insights on the volume-conservative time-fractional Allen-Cahn equation compared with the non-volume-preserving one and Cahn-Hilliard equation.

2 Time-fractional phase field models

Introduce a phase variable ϕ , for the effective free energy of the phase model $E[\phi]$,

$$E[\phi] = \int_{\Omega} \left(\frac{\varepsilon^2}{2} |\nabla \phi|^2 + F(\phi) \right) d\mathbf{x}, \quad F(\phi) = \frac{1}{4} (1 - \phi^2)^2, \quad (2.1)$$

in which ε is a parameter describing the width of the interface, the time-fractional Allen-Cahn equation then reads

$$\partial_t^\alpha \phi = -\lambda \frac{\delta E}{\delta \phi}, \quad (2.2)$$

where positive constant λ is the mobility parameter, $\frac{\delta E}{\delta \phi}$ is the functional derivative of E with respect to phase variable ϕ . Here, the notation $\partial_t^\alpha := {}^C D_t^\alpha$ in (2.2) denotes the Caputo's fractional derivative of order α with respect to t , i.e.,

$$(\partial_t^\alpha v)(t) := (\mathcal{I}_t^{1-\alpha} v')(t) = \int_0^t \omega_{1-\alpha}(t-s) v'(s) ds, \quad 0 < \alpha < 1, \quad (2.3)$$

involving the fractional Riemann-Liouville integral \mathcal{I}_t^β of order $\beta > 0$, that is,

$$(\mathcal{I}_t^\beta v)(t) := \int_0^t \omega_\beta(t-s) v(s) ds, \quad \text{where} \quad \omega_\beta(t) := t^{\beta-1} / \Gamma(\beta). \quad (2.4)$$

It is remarkable that, in comparison with the energy dissipation law of the local Allen-Cahn model, Tang et al. [19] proved that the energy stable property of the nonlocal one is given by,

$$E[\phi(T)] - E[\phi(0)] = -\frac{1}{\lambda} \int_\Omega \mathcal{I}_t^1 (\partial_t \phi \mathcal{I}_t^{1-\alpha} \partial_t \phi)(T) d\mathbf{x} \leq 0. \quad (2.5)$$

The non-positive of the right part of above relation is determined by [19, Lemma 2.1].

Evidently, acting the Riemann-Liouville fractional derivative ${}^{RL} D_t^{1-\alpha}$ on both sides of equation (2.2), and using the identity ${}^{RL} D_t^{1-\alpha} {}^C D_t^\alpha v(s) = v'(s)$, one has the following relation

$$\frac{d}{dt} \int_\Omega \phi d\mathbf{x} = -\lambda {}^{RL} D_t^{1-\alpha} \int_\Omega \frac{\delta E}{\delta \phi} d\mathbf{x} \neq 0, \quad (2.6)$$

which means the time-fractional Allen-Cahn equation does not preserve the initial volume that is consistent with the integer order one. In order to impose the conservation of volume

$$\int_\Omega \phi(\mathbf{x}, t) d\mathbf{x} = \int_\Omega \phi(\mathbf{x}, 0) d\mathbf{x}, \quad (2.7)$$

and without influencing the original energy stable property (2.5), inspired by the volume conservation integer order Allen-Cahn equation performed in [6], the equation (2.2) is modified by adding a nonlocal time-dependent Lagrange multiplier $\eta(t)$ as follows

$$\partial_t^\alpha \phi = -\lambda \left(\frac{\delta E}{\delta \phi} - \eta(t) \right), \quad (2.8)$$

where the expression of the new term is given by $\eta(t) = \frac{1}{|\Omega|} \int_\Omega \frac{\delta E}{\delta \phi} d\mathbf{x}$ for the necessary condition to guarantee the invariant volume, i.e.,

$$\frac{d}{dt} \int_\Omega \phi d\mathbf{x} = -\lambda {}^{RL} D_t^{1-\alpha} \int_\Omega \left(\frac{\delta E}{\delta \phi} - \eta(t) \right) d\mathbf{x} = 0. \quad (2.9)$$

As well-known, based upon the free energy $E[\phi]$, another model that maintains the initial volume is the time-fractional Cahn-Hilliard equation [19],

$$\partial_t^\alpha \phi = \lambda \Delta \frac{\delta E}{\delta \phi}. \quad (2.10)$$

After a small calculation analogous to the derivation of (2.6), we see that

$$\frac{d}{dt} \int_{\Omega} \phi \, d\mathbf{x} = \lambda_0^{RL} D_t^{1-\alpha} \int_{\Omega} \Delta \frac{\delta E}{\delta \phi} \, d\mathbf{x} = 0, \quad (2.11)$$

where the periodic boundary condition is chosen to ensure that the boundary integrals vanish. Meanwhile, the model (2.10) preserves the energy stable property,

$$E[\phi(T)] - E[\phi(0)] = -\frac{1}{\lambda} \int_{\Omega} \mathcal{I}_t^1 (\nabla \psi \mathcal{I}_t^{1-\alpha} \nabla \psi)(T) \, d\mathbf{x} \leq 0, \quad (2.12)$$

in which $\psi = -\Delta^{-1} \partial_t \phi$ is the solution of the equation $-\Delta \psi = \partial_t \phi$ with periodic boundary condition, see [19, Lemma 2.3] for more details.

To our knowledge, for the above time-fractional phase field models, there are limited results in the literature on numerical approaches preserving the discrete volume conservation as well as energy dissipation law, especially on nonuniform time grids. Therefore the first objective of this paper is to build nonuniform time-stepping methods for the continuous systems to inherit the corresponding invariant or dissipative properties enjoyed by the original systems.

We consider the nonuniform time levels $0 = t_0 < t_1 < \dots < t_{k-1} < t_k < \dots < t_N = T$ with the time-step sizes $\tau_k := t_k - t_{k-1}$ for $1 \leq k \leq N$ and the maximum time-step size $\tau := \max_{1 \leq k \leq N} \tau_k$. Also, let the local time-step ratio $\rho_k := \tau_k / \tau_{k+1}$ and the maximum step ratio $\rho := \max_{k \geq 1} \rho_k$. Given a grid function $\{v^k\}$, put $\nabla_{\tau} v^k := v^k - v^{k-1}$, $\partial_{\tau} v^{k-\frac{1}{2}} := \nabla_{\tau} v^k / \tau_k$ and $v^{k-\frac{1}{2}} := (v^k + v^{k-1})/2$ for $k \geq 1$. Always, let $(\Pi_{1,k} v)(t)$ denote the linear interpolant of a function $v(t)$ at two nodes t_{k-1} and t_k , and define a piecewise linear approximation

$$\Pi_1 v := \Pi_{1,k} v \quad \text{so that} \quad (\Pi_1 v)'(t) = \partial_{\tau} v^{k-\frac{1}{2}} \quad \text{for } t_{k-1} < t \leq t_k \text{ and } k \geq 1. \quad (2.13)$$

To reveal the initial singularity of solution of the time-fractional phase field models, we apply the $L1^+$ formula that we see shortly to the time-fractional problem (2.8), and more details can be found in subsection 3.1 and Example 4.2. The drawings in Figure 1 depict the discrete time derivative $\partial_{\tau} \phi^{k-\frac{1}{2}}$ near $t = 0$ on the graded mesh $t_k = (k/N)^{\gamma}$ when fractional order $\alpha = 0.7$. The numerical results suggest that

$$\log |\phi_t(\mathbf{x}, t)| \approx (\alpha - 1) \log(t) + C(\mathbf{x}) \quad \text{as } t \rightarrow 0,$$

and tell us that the solution is weakly singularity like $\phi_t = O(t^{\alpha-1})$ near initial time, which could be alleviated by using the graded mesh. Hence, the second objective of present work is to resolve the essentially weak singularity in the time-fractional phase field by refining time mesh.

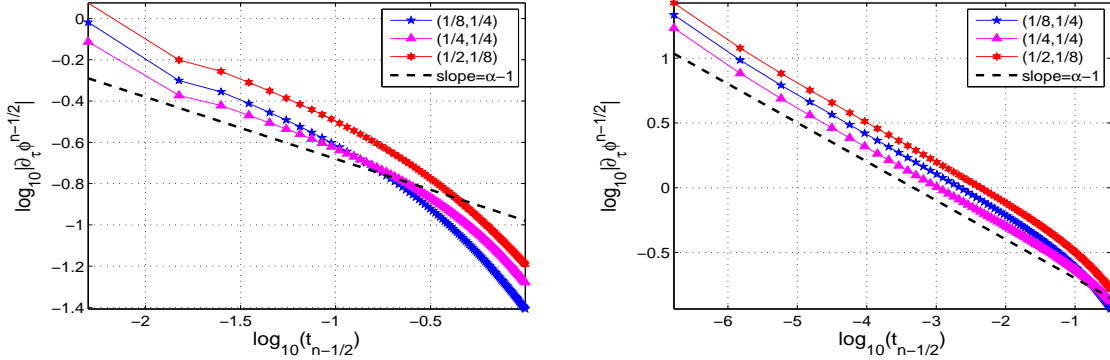


Figure 1: The log-log plot of the difference quotient $\partial_\tau \phi^{k-\frac{1}{2}}$ versus time for problem (2.8) with fractional order $\alpha = 0.7$ and $\gamma = 1, 3$ (from left to right), respectively.

3 Energy stable numerical approaches

To achieve the above assertions, our starting point is to apply the $L1^+$ formula to approximate the Caputo derivative, which naturally possesses the energy dissipation property on nonuniform time levels when it is applied to the time-fractional phased filed models.

3.1 The $L1^+$ formula of Caputo derivative

The $L1^+$ formula for the Caputo derivative (2.3) is defined at time $t = t_{n-\frac{1}{2}}$ as follows

$$(\partial_\tau^\alpha v)^{n-\frac{1}{2}} := \frac{1}{\tau_n} \int_{t_{n-1}}^{t_n} \int_0^t \omega_{1-\alpha}(t-s)(\Pi_1 v)'(s) ds dt = \sum_{k=1}^n a_{n-k}^{(n)} \nabla_\tau v^k \quad \text{for } n \geq 1, \quad (3.1)$$

in which the discrete convolution kernels $a_{n-k}^{(n)}$ are given by

$$a_{n-k}^{(n)} := \frac{1}{\tau_n \tau_k} \int_{t_{n-1}}^{t_n} \int_{t_{k-1}}^{\min\{t, t_k\}} \omega_{1-\alpha}(t-s) ds dt \quad \text{for } 1 \leq k \leq n. \quad (3.2)$$

Following the discussions given in [22, Lemma 3.1], we have the following remarkable property. It says that the $L1^+$ formula is positive semi-definite on arbitrary nonuniform meshes.

Lemma 3.1 *The discrete convolution kernels $a_{n-k}^{(n)}$ in (3.2) are positive and positive semi-definite. For any real sequence $\{w_k\}_{k=1}^n$ with n entries, it holds that*

$$\sum_{k=1}^n w_k \sum_{j=1}^k a_{k-j}^{(k)} w_j \geq 0 \quad \text{for } n \geq 1.$$

The definition (3.2) of discrete kernels $a_j^{(n)}$ and the integral mean-value theorem yield the following result.

Lemma 3.2 *The positive discrete kernels $a_{n-k}^{(n)}$ in (3.2) fulfill*

$$a_0^{(n)} = \frac{1}{\Gamma(3-\alpha)\tau_n^\alpha}, \quad a_1^{(n)} > a_2^{(n)} > \dots > a_{n-1}^{(n)} > 0 \quad \text{for } n \geq 2.$$

Simple manipulations of the first two discrete kernels reveal that

$$a_0^{(n)} - a_1^{(n)} = \frac{1}{\Gamma(3-\alpha)\tau_n^\alpha \rho_{n-1}} (1 + \rho_{n-1} + \rho_{n-1}^{2-\alpha} - (1 + \rho_{n-1})^{2-\alpha}).$$

It is easily seen that $a_0^{(n)} < a_1^{(n)}$ as $\alpha \rightarrow 0$ and $a_0^{(n)} > a_1^{(n)}$ as $\alpha \rightarrow 1$, that is, the value of $a_0^{(n)} - a_1^{(n)}$ may change the sign when the fractional order α varies over $(0, 1)$.

It is to mention that, the nonuniform L1⁺ formula is quite different from some nonuniform formulas approximating the Caputo time derivative, including the L1 formula [25, 26], L1-2_σ (Alikhanov) formula [27, 28], and Caputo's BDF2-type formula [29]. We compare them in Table 1, in which the discrete kernels are referred to the sequence $\{A_{n-k}^{(n)}\}$ in the form $\sum_{k=1}^n A_{n-k}^{(n)} \nabla_\tau v^n$ or $\sum_{k=1}^n A_k^{(n)} \nabla_\tau v^{n-k}$. As seen, the L1⁺ formula has some advantages: it is second-order accuracy, the convergence order is independent of the fractional order α , and is positive semi-definite in the sense of Lemma 3.1. Actually, these properties make it useful in designing linear, second-order energy stable schemes to the time-fractional phase field models introduced in Section 2.

Table 1: Numerical Caputo derivatives on nonuniform meshes.

Numerical Formula	L1 [25, 26]	Alikhanov [27, 28]	CBDF2 [29]	L1 ⁺ [22]
Formal accuracy	$2 - \alpha$	$3 - \alpha$	$3 - \alpha$	2
Positive kernels	Yes	Yes	$A_1^{(n)} \not\geq 0$	Yes
Monotonous kernels	Yes	Yes	$A_1^{(n)} \not\geq A_2^{(n)}$	$A_0^{(n)} \not\geq A_1^{(n)}$
Positive semi-definite	Unknown	Unknown	Unknown	Yes

3.2 Numerical approach using IEQ

For the volume-conserving time-fractional Allen-Cahn model (2.8), we introduce an auxiliary function $u(\phi)$ in term of original variable ϕ given by

$$u(\phi) = \phi^2 - 1 - \beta, \quad (3.3)$$

where the artificial parameter β is utilized to regularize the numerical approaches. As a consequence, the free energy of the original problem is transformed into a quadratic form

$$E[\phi, u] = \int_{\Omega} \left(\frac{\varepsilon^2}{2} |\nabla \phi|^2 + \frac{\beta}{2} |\phi|^2 + \frac{1}{4} u^2 \right) \mathrm{d}\mathbf{x} - \left(\frac{\beta}{2} + \frac{\beta^2}{4} \right) |\Omega|. \quad (3.4)$$

Correspondingly, the problem (2.8) could be reformulated to the following equivalent form

$$\partial_t^\alpha \phi = -\lambda \left(-\varepsilon^2 \Delta \phi + \beta \phi + u \phi - \eta \right), \quad (3.5)$$

$$\eta = \frac{1}{|\Omega|} \int_{\Omega} (-\varepsilon^2 \Delta \phi + \beta \phi + u \phi) \, d\mathbf{x}, \quad (3.6)$$

$$\partial_t u = 2\phi \partial_t \phi. \quad (3.7)$$

The new system is subjected to the initial conditions

$$\phi(\mathbf{x}, 0) = \phi_0(\mathbf{x}) \quad \text{and} \quad u(0) = u(\phi_0(\mathbf{x})), \quad (3.8)$$

and the same boundary conditions of the primitive model. Define the usual L^2 inner product $(f, g) = \int_{\Omega} f g \, d\mathbf{x}$ for all $f, g \in L^2(\Omega)$. We see clearly that the equivalent system preserves the volume-preserving property (2.7) by making the L^2 inner product of (3.5) with a constant and finding that $(\partial_t^\alpha \phi, 1) = 0$. Also, taking the inner product of (3.5) and (3.7) with $\partial_t \phi$ and u respectively, summing up the resulting equalities, and integrating the time t from $t = 0$ to T , we obtain the energy decay law

$$E[\phi(T), u(T)] - E[\phi(0), u(0)] = -\frac{1}{\lambda} \int_{\Omega} \mathcal{I}_t^1 (\partial_t \phi \mathcal{I}_t^{1-\alpha} \partial_t \phi)(T) \, d\mathbf{x} \leq 0, \quad (3.9)$$

where we use the fact $(\eta, \partial_t \phi) = 0$ due to the condition (2.9).

By virtue of the equivalent PDE system (3.5)-(3.7), we construct new numerical schemes that concern only with the time discretization, while the spatial approximations can be diverse, examples as finite difference, finite element or spectral methods. Integrating the equations (3.5)-(3.7) from $t = t_{n-1}$ to t_n , respectively, results in the following equations

$$\frac{1}{\tau_n} \int_{t_{n-1}}^{t_n} \partial_t^\alpha \phi \, dt = -\frac{\lambda}{\tau_n} \int_{t_{n-1}}^{t_n} (-\varepsilon^2 \Delta \phi + \beta \phi + u \phi - \eta) \, dt, \quad (3.10)$$

$$\frac{1}{\tau_n} \int_{t_{n-1}}^{t_n} \eta \, dt = \frac{1}{|\Omega| \tau_n} \int_{t_{n-1}}^{t_n} \int_{\Omega} (-\varepsilon^2 \Delta \phi + \beta \phi + u \phi) \, d\mathbf{x} \, dt, \quad (3.11)$$

$$\frac{1}{\tau_n} \int_{t_{n-1}}^{t_n} \partial_t u \, dt = \frac{2}{\tau_n} \int_{t_{n-1}}^{t_n} \phi \partial_t \phi \, dt. \quad (3.12)$$

By means of the $L1^+$ formula (3.1), the trapezoidal formula, we have the following Crank-Nicolson IEQ (CN-IEQ) time-stepping scheme

$$(\partial_\tau^\alpha \phi)^{n-\frac{1}{2}} = -\lambda \left(-\varepsilon^2 \Delta \phi^{n-\frac{1}{2}} + \beta \phi^{n-\frac{1}{2}} + u^{n-\frac{1}{2}} \hat{\phi}^{n-\frac{1}{2}} - \eta^{n-\frac{1}{2}} \right), \quad (3.13)$$

$$\eta^{n-\frac{1}{2}} = \frac{1}{|\Omega|} \int_{\Omega} \left(-\varepsilon^2 \Delta \phi^{n-\frac{1}{2}} + \beta \phi^{n-\frac{1}{2}} + u^{n-\frac{1}{2}} \hat{\phi}^{n-\frac{1}{2}} \right) \, d\mathbf{x}, \quad (3.14)$$

$$\partial_\tau u^{n-\frac{1}{2}} = 2\hat{\phi}^{n-\frac{1}{2}} \partial_\tau \phi^{n-\frac{1}{2}}, \quad (3.15)$$

where $\hat{\phi}^{n-\frac{1}{2}} := \phi^{n-1} + \nabla_\tau \phi^{n-1} / (2\rho_{n-1})$ is the local extrapolation.

Theorem 3.1 *The CN-IEQ scheme (3.13)-(3.15) conserves the volume,*

$$\int_{\Omega} \phi^n \, d\mathbf{x} = \int_{\Omega} \phi^{n-1} \, d\mathbf{x}, \quad \text{for } 1 \leq n \leq N. \quad (3.16)$$

Proof We prove the discrete volume-conserving by induction. It is easy to check that the volume conservation holds when $n = 1$. In what follows, we assume that the relation (3.16) is valid for the numerical scheme (3.13)-(3.15) with no more than $(N - 1)$ indices, where $N \geq 2$. It is sufficient to verify the desired assertion still holds for $n = N$. Actually, we have

$$\begin{aligned} \left(a_0^{(n)} \nabla_\tau \phi^n, 1 \right) &= \left((\partial_\tau^\alpha \phi)^{n-\frac{1}{2}}, 1 \right) \\ &= -\lambda \left(-\varepsilon^2 \Delta \phi^{n-\frac{1}{2}} + \beta \phi^{n-\frac{1}{2}} + u^{n-\frac{1}{2}} \hat{\phi}^{n-\frac{1}{2}} - \eta^{n-\frac{1}{2}}, 1 \right) = 0, \end{aligned} \quad (3.17)$$

where the induction assumption $(\phi^n, 1) = (\phi^{n-1}, 1)$, $1 \leq n \leq N - 1$ has been used in the derivation of the above identity. We then have $(\phi^N, 1) = (\phi^{N-1}, 1)$ that shows the desired result still holds for $n = N$. Consequently, the relationship (3.16) is valid by the induction. \blacksquare

Note that, the remarkable property of $L1^+$ formula in Lemma 3.1 implies that the above CN-IEQ scheme (3.13)-(3.15) is naturally suitable for a general class of nonuniform time meshes. Precisely, the following result shows that it is unconditionally energy stable.

Theorem 3.2 *The CN-IEQ scheme (3.13)-(3.15) preserves the energy dissipation law,*

$$E[\phi^n, u^n] - E[\phi^0, u^0] \leq 0, \quad \text{for } 1 \leq n \leq N, \quad (3.18)$$

such that it is unconditionally stable, where discrete energy is given by

$$E[\phi^n, u^n] = \int_{\Omega} \left(\frac{\varepsilon^2}{2} |\nabla \phi^n|^2 + \frac{\beta}{2} |\phi^n|^2 + \frac{1}{4} (u^n)^2 \right) dx - \left(\frac{\beta}{2} + \frac{\beta^2}{4} \right) |\Omega|.$$

Proof Taking the inner product of (3.13) and (3.15) with $\nabla_\tau \phi^n$ and $2\tau_n u^{n-\frac{1}{2}}$, respectively, and adding the resulting two equalities, we have the following equation

$$-\frac{1}{\lambda} \left((\partial_\tau^\alpha \phi)^{n-\frac{1}{2}}, \nabla_\tau \phi^n \right) = \left(-\varepsilon^2 \Delta \phi^{n-\frac{1}{2}} + \beta \phi^{n-\frac{1}{2}}, \nabla_\tau \phi^n \right) + \frac{1}{4} \left((u^n)^2 - (u^{n-1})^2, 1 \right), \quad (3.19)$$

in which the volume conservation (3.16) has been used to show the fact $(\eta^{n-\frac{1}{2}}, \nabla_\tau \phi^n) = 0$. As a result, we get the following identity

$$E[\phi^k, u^k] - E[\phi^{k-1}, u^{k-1}] = -\frac{1}{\lambda} \left((\partial_\tau^\alpha \phi)^{k-\frac{1}{2}}, \nabla_\tau \phi^k \right) \quad \text{for } 1 \leq k \leq n. \quad (3.20)$$

By summing the superscript k from 1 to n , we obtain the following inequality

$$E[\phi^n, u^n] - E[\phi^0, u^0] = -\frac{1}{\lambda} \int_{\Omega} \sum_{k=1}^n \nabla_\tau \phi^k \sum_{j=1}^k a_{k-j}^{(k)} \nabla_\tau \phi^k dx \leq 0 \quad \text{for } 1 \leq n \leq N.$$

where Lemma 3.1 has been used in the last inequality. It completes the proof. \blacksquare

3.3 Numerical approach using SAV

For the time-fractional Allen-Cahn model with volume constraint (2.8), we here introduce a scalar auxiliary function $v(t)$ in term of original variable ϕ as follows

$$v(t) = \sqrt{\int_{\Omega} \frac{1}{4} (\phi^2 - 1 - \beta)^2 d\mathbf{x} + C_0}, \quad (3.21)$$

where the positive constant C_0 is chosen to ensure the radicand positive and β is the regularized parameter. Therefore, the free energy of the primitive problem could be rewritten into

$$E[\phi, v] = \int_{\Omega} \left(\frac{\varepsilon^2}{2} |\nabla \phi|^2 + \frac{\beta}{2} |\phi|^2 \right) d\mathbf{x} + v^2 - C_0 - \left(\frac{\beta}{2} + \frac{\beta^2}{4} \right) |\Omega|. \quad (3.22)$$

We then could reformulate the problem (2.8) as an equivalent form

$$\partial_t^\alpha \phi = -\lambda (-\varepsilon^2 \Delta \phi + \beta \phi + V(\phi)v - \eta), \quad (3.23)$$

$$\eta = \frac{1}{|\Omega|} \int_{\Omega} (-\varepsilon^2 \Delta \phi + \beta \phi + V(\phi)v) d\mathbf{x}, \quad (3.24)$$

$$v_t = \frac{1}{2} \int_{\Omega} V(\phi) \partial_t \phi d\mathbf{x}, \quad (3.25)$$

in which the expression of the notation $V(\phi)$ is given by

$$V(\phi) = \frac{(\phi^2 - 1 - \beta)\phi}{\sqrt{\int_{\Omega} \frac{1}{4} (\phi^2 - 1 - \beta)^2 d\mathbf{x} + C_0}}, \quad (3.26)$$

with the following initial conditions

$$\phi(\mathbf{x}, 0) = \phi_0(\mathbf{x}) \quad \text{and} \quad v(0) = v(\phi_0(\mathbf{x})). \quad (3.27)$$

It is easy to check that the new system admits the volume-conserving property (2.7) and the following energy dissipation law

$$E[\phi(T), v(T)] - E[\phi(0), v(0)] = -\frac{1}{\lambda} \int_{\Omega} \mathcal{I}_t^1 (\partial_t \phi \mathcal{I}_t^{1-\alpha} \partial_t \phi)(T) d\mathbf{x} \leq 0. \quad (3.28)$$

As done in the above subsection, for the equivalent system (3.23)-(3.25), we have the following Crank-Nicolson SAV (CN-SAV) scheme

$$(\partial_\tau^\alpha \phi)^{n-\frac{1}{2}} = -\lambda \left(-\varepsilon^2 \Delta \phi^{n-\frac{1}{2}} + \beta \phi^{n-\frac{1}{2}} + V(\hat{\phi}^{n-\frac{1}{2}}) v^{n-\frac{1}{2}} - \eta^{n-\frac{1}{2}} \right), \quad (3.29)$$

$$\eta^{n-\frac{1}{2}} = \frac{1}{|\Omega|} \int_{\Omega} \left(-\varepsilon^2 \Delta \phi^{n-\frac{1}{2}} + \beta \phi^{n-\frac{1}{2}} + V(\hat{\phi}^{n-\frac{1}{2}}) v^{n-\frac{1}{2}} \right) d\mathbf{x}, \quad (3.30)$$

$$\partial_\tau v^{n-\frac{1}{2}} = \frac{1}{2} \int_{\Omega} V(\hat{\phi}^{n-\frac{1}{2}}) \partial_\tau \phi^{n-\frac{1}{2}} d\mathbf{x}, \quad (3.31)$$

Also, we have the following theorems on the volume conservation and energy dissipation by following the proofs of Theorems 3.1 and 3.2, respectively.

Theorem 3.3 *The CN-SAV scheme (3.29)-(3.31) inherits the volume conservation,*

$$\int_{\Omega} \phi^n \, d\mathbf{x} = \int_{\Omega} \phi^{n-1} \, d\mathbf{x}, \quad \text{for } 1 \leq n \leq N. \quad (3.32)$$

Theorem 3.4 *The CN-IEQ scheme (3.29)-(3.31) preserves the energy dissipation law,*

$$E[\phi^n, v^n] - E[\phi^0, v^0] \leq 0, \quad \text{for } 1 \leq n \leq N, \quad (3.33)$$

such that it is unconditionally stable, in which

$$E[\phi^n, v^n] = \int_{\Omega} \left(\frac{\varepsilon^2}{2} |\nabla \phi^n|^2 + \frac{\beta}{2} |\phi^n|^2 \right) d\mathbf{x} + (v^n)^2 - C_0 - \left(\frac{\beta}{2} + \frac{\beta^2}{4} \right) |\Omega|.$$

3.4 Numerical approaches for the time-fractional Cahn-Hilliard model

In order to make a comparison study between the two volume-preserving models (2.8) and (2.10), we include the CN-IEQ scheme for time-fractional Cahn-Hilliard equation (2.10)

$$\begin{aligned} (\partial_{\tau}^{\alpha} \phi)^{n-\frac{1}{2}} &= \lambda \Delta \left(-\varepsilon^2 \Delta \phi^{n-\frac{1}{2}} + \beta \phi^{n-\frac{1}{2}} + q^{n-\frac{1}{2}} \hat{\phi}^{n-\frac{1}{2}} \right), \\ \partial_{\tau} q^{n-\frac{1}{2}} &= 2 \hat{\phi}^{n-\frac{1}{2}} \partial_{\tau} \phi^{n-\frac{1}{2}}, \end{aligned}$$

in which $q(\phi) = \phi^2 - 1 - \beta$, and the following CN-SAV scheme

$$\begin{aligned} (\partial_{\tau}^{\alpha} \phi)^{n-\frac{1}{2}} &= \lambda \Delta \left(-\varepsilon^2 \Delta \phi^{n-\frac{1}{2}} + \beta \phi^{n-\frac{1}{2}} + R(\hat{\phi}^{n-\frac{1}{2}}) r^{n-\frac{1}{2}} \right), \\ \partial_{\tau} r^{n-\frac{1}{2}} &= \frac{1}{2} \int_{\Omega} R(\hat{\phi}^{n-\frac{1}{2}}) \partial_{\tau} \phi^{n-\frac{1}{2}} \, d\mathbf{x}, \end{aligned}$$

where

$$r(t) = \sqrt{\int_{\Omega} \frac{1}{4} (\phi^2 - 1 - \beta)^2 + C_0}, \quad R(\phi) = \frac{(\phi^2 - 1 - \beta) \phi}{\sqrt{\int_{\Omega} \frac{1}{4} (\phi^2 - 1 - \beta)^2 \, d\mathbf{x} + C_0}}.$$

It is not difficult to show that the two computationally efficient approaches both are volume-conserving and unconditionally energy stable by following the proofs of Theorems 3.1 or 3.2, but we here omit the details for brevity.

4 Adaptive time-stepping and examples

The CN-IEQ scheme (3.13)-(3.15) and CN-SAV scheme (3.29)-(3.31) are run for the conservative time-fractional Allen-Cahn model (2.8) in this section. Always, we adopt the fast algorithm to speed up the evaluation of the $L1^+$ formula by setting an absolute tolerance error $\epsilon = 10^{-12}$ for the underlying SOE approximation, see [22]. The spatial domain Ω is divided uniformly using an equispaced mesh in each direction and the Fourier pseudo-spectral method is employed.

Also, to compensate the lack of smoothness of the solution, the time interval $[0, T]$ is always divided into two parts $[0, T_0]$ and $[T_0, T]$ with total N subintervals. Take the graded parameter

$\gamma \geq 1$ and apply the graded mesh $t_k = T_0(k/N_0)^\gamma$ in $[0, T_0]$ to resolve the initial singularity. Some different time-stepping approaches are examined in the remainder interval $[T_0, T]$. In the following context, the *Graded Step* strategy uses the graded mesh in the starting cell $[0, T_0]$ with the uniform mesh in the remainder interval $(T_0, T]$; while the *Adaptive Step* strategy employs the graded mesh in $[0, T_0]$ and use certain adaptive time-stepping approach described below in the remainder interval $(T_0, T]$.

4.1 Adaptive time-stepping strategy

To resolve the time evolutions accurately, small time steps are always necessary to capture the fast dynamics; but the computations would become quite costly for the coarsening process, see the initial random perturbation problems in Example 4.3. Fortunately, the proposed numerical schemes are proven in Section 3 to be unconditionally energy stable and allow large time steps to reduce the computation cost for the coarsening process. Thus some adaptive time-stepping strategy is useful to resolve the widely varying time scales and significantly reduce the computational cost. In current computations, we adjust the size of time step using the formula [30],

$$\tau_{ada} = \max \left\{ \tau_{\min}, \frac{\tau_{\max}}{\sqrt{1 + \kappa |E'(t)|^2}} \right\}. \quad (4.1)$$

Here the parameters τ_{\max}, τ_{\min} refer to the predetermined maximum and minimum time steps, as well as κ is chosen by the user to adjust the level of adaptivity.

4.2 Accuracy verification

The numerical accuracy in time of our CN-IEQ and CN-SAV schemes is examined by taking $T_0 = \min\{1/\gamma, T\}$ and using the *random* mesh in the remainder time interval $(T_0, T]$, that is, $\tau_{N_0+k} := (T - T_0)\epsilon_k/S_1$ for $1 \leq k \leq N_1 := N - N_0$, where $S_1 = \sum_{k=1}^{N_1} \epsilon_k$ and $\epsilon_k \in (0, 1)$ are the random numbers. The maximum norm error $e(N) := \max_{1 \leq n \leq N} \|U^n - u^n\|_\infty$ is recorded in each run and the experimental order of convergence is computed by

$$\text{Order} \approx \frac{\log(e(N)/e(2N))}{\log(\tau(N)/\tau(2N))}$$

in which $\tau(N)$ denotes the maximum time-step size for total N subintervals.

Table 2: Numerical accuracy of CN-IEQ scheme (3.13)-(3.15) with $\alpha = 0.8, \sigma = 0.4$

N	τ	$\gamma = 2$		τ	$\gamma = 5$		τ	$\gamma = 6$	
		$e(N)$	Order		$e(N)$	Order		$e(N)$	Order
10	1.72e-01	2.41e-02	—	2.69e-01	2.44e-02	—	2.69e-01	3.08e-02	—
20	1.00e-01	1.38e-02	1.02	1.24e-01	4.59e-03	2.17	1.31e-01	6.42e-03	2.18
40	5.39e-02	8.50e-03	0.79	1.07e-02	3.46e-05	2.00	6.75e-02	1.45e-03	2.24
80	3.07e-02	5.22e-03	0.87	3.49e-02	3.16e-04	1.90	3.33e-02	3.13e-04	2.18

Table 3: Numerical accuracy of CN-SAV scheme (3.29)-(3.31) with $\alpha = 0.8$, $\sigma = 0.4$

N	τ	$\gamma = 2$		τ	$\gamma = 5$		τ	$\gamma = 6$	
		$e(N)$	Order		$e(N)$	Order		$e(N)$	Order
10	1.86e-01	2.40e-02	—	3.23e-01	1.86e-02	—	2.88e-01	2.33e-02	—
20	1.02e-01	1.38e-02	0.92	1.34e-01	2.99e-03	2.08	1.27e-01	6.78e-03	1.51
40	5.31e-02	8.51e-03	0.74	6.95e-02	1.06e-03	1.57	6.08e-02	9.51e-04	2.66
80	2.76e-02	5.22e-03	0.75	3.83e-02	3.16e-04	2.03	3.36e-02	2.55e-04	2.21

Example 4.1 Consider the model $\partial_t^\alpha \phi = -\frac{\delta E}{\delta \phi} + \eta(t) + g(\mathbf{x}, t)$ with $\varepsilon^2 = 0.5$ for $\mathbf{x} \in (0, 2\pi)^2$ and $0 < t < 1$ such that it has an exact solution $\phi = \omega_{1+\sigma}(t) \sin(x) \sin(y)$.

The spatial domain is discretized by using 128×128 meshes. We chose the fractional order $\alpha = 0.8$, the regular parameter $\sigma = 0.4$ and the artificial parameters $\beta = 1$ and $C_0 = 1$. Tables 2 and 3 list the numerical results of CN-IEQ and CN-SAV approaches with different graded parameters γ . It is seen that the time accuracy is of order $O(\tau^{\gamma\sigma})$ when $\gamma < 2/\sigma$, and the second-order accuracy is achieved when $\gamma \geq \gamma_{\text{opt}} = 2/\sigma$. They suggest that the time accuracy is about of $O(\tau^{\min\{\gamma\sigma, 2\}})$ in time although no theoretical proof is available up to now.

4.3 Numerical comparisons

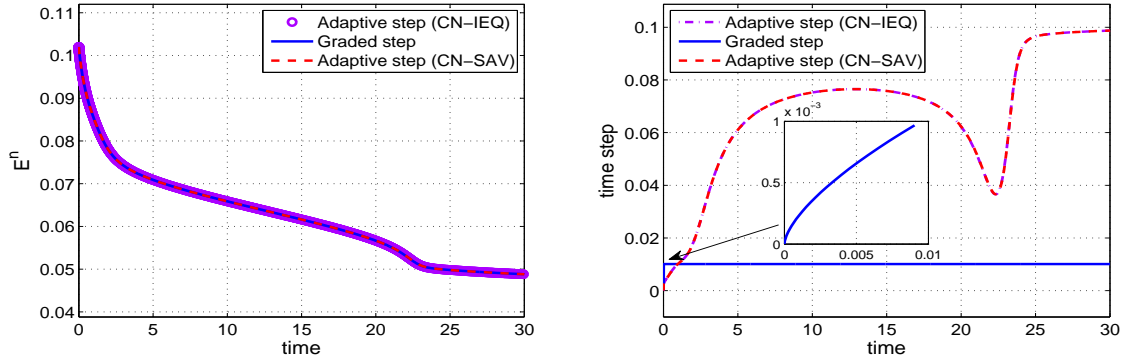


Figure 2: Evolutions of energy (left) and time steps (right) of the conservative time-fractional Allen-Cahn equation using different time strategies until final time $T = 30$.

Example 4.2 Consider three different phase field models, covering time-fractional Allen-Cahn, the conservative version and time-fractional Cahn-Hilliard equations, with the coefficients $\lambda = 1$ and $\varepsilon = 0.02$. The CN-IEQ and CN-SAV methods with the parameters $\beta = 4$ and $C_0 = 1$ are applied to simulate the merging of four drops with an initial condition

$$\begin{aligned} \phi_0(\mathbf{x}) = & -\tanh\left(\left((x-0.3)^2 + y^2 - 0.2^2\right)/\varepsilon\right) \tanh\left(\left((x+0.3)^2 + y^2 - 0.2^2\right)/\varepsilon\right) \\ & \times \tanh\left(\left(x^2 + (y-0.3)^2 - 0.2^2\right)/\varepsilon\right) \tanh\left(\left(x^2 + (y+0.3)^2 - 0.2^2\right)/\varepsilon\right). \end{aligned} \quad (4.2)$$

The computational domain $\Omega = (-1, 1)^2$ is divided uniformly into 128 parts in each direction.

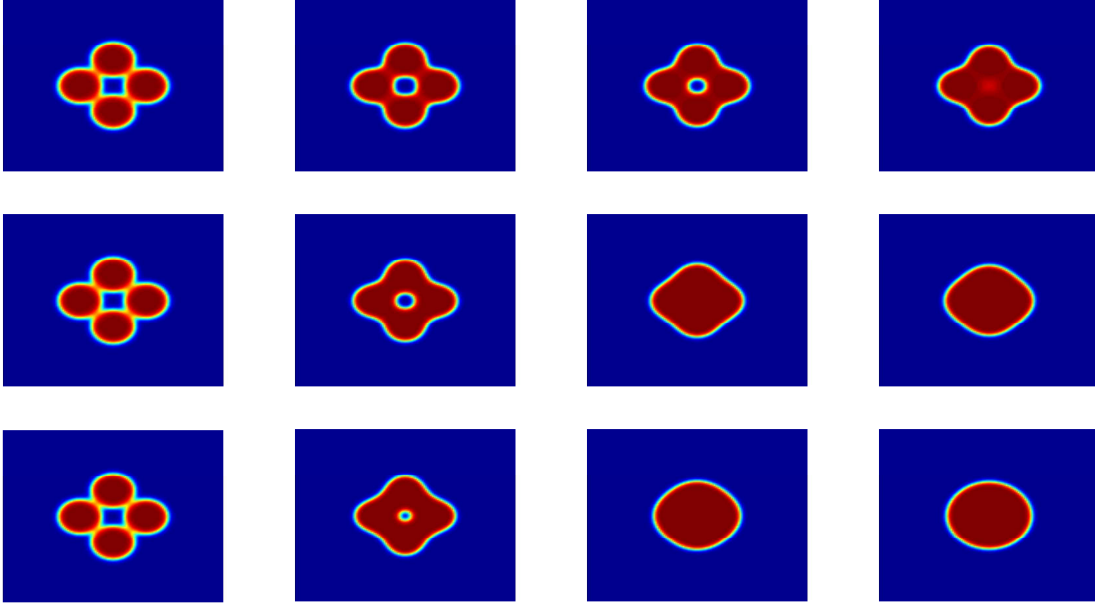


Figure 3: Solution snapshots at $t = 1, 30, 100, 200$ (from left to right) for three fractional orders $\alpha = 0.4, 0.7$ and 0.9 (from top to bottom), respectively.

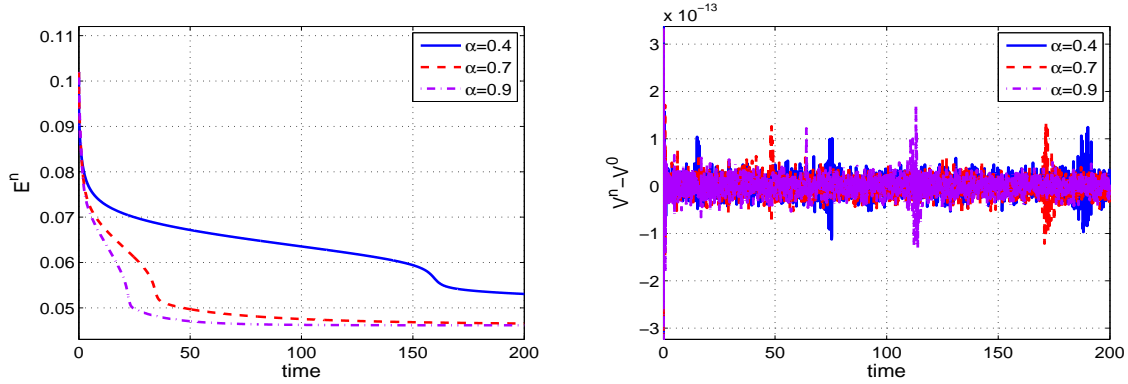


Figure 4: Evolutions of energy and volume curves (from left to right) for the conservative time-fractional Allen-Cahn equation with fractional order $\alpha = 0.4, 0.7$ and 0.9 , respectively.

We examine different time-stepping approaches for simulating the model (2.8) until the final time $T = 30$ with a fractional order $\alpha = 0.9$. Always, put $T_0 = 0.01$, $N_0 = 30$ and $\gamma = 3$ in the starting cell $[0, T_0]$. We consider the *Grade Step* approach using the uniform mesh with $N_1 = 2970$, and the *Adaptive Step* approach with parameters $\kappa = 10^6$, $\tau_{\min} = \tau_{N_0} = 10^{-3}$ and $\tau_{\max} = 10^{-1}$. From Figure 2, the discrete energy curves generated by using the adaptive time steps practically coincide with those by *Grade Step* approach, for both the CN-IEQ and CN-SAV methods. As expected, the *Adaptive Step* approach uses small time steps when the energy dissipates fast, and generates large time steps otherwise. In the remainder interval $(T_0, T]$, we put 2970 points on the uniform mesh, while the total number of adaptive time steps are 667. So the adaptive time-stepping strategy is computationally efficient.

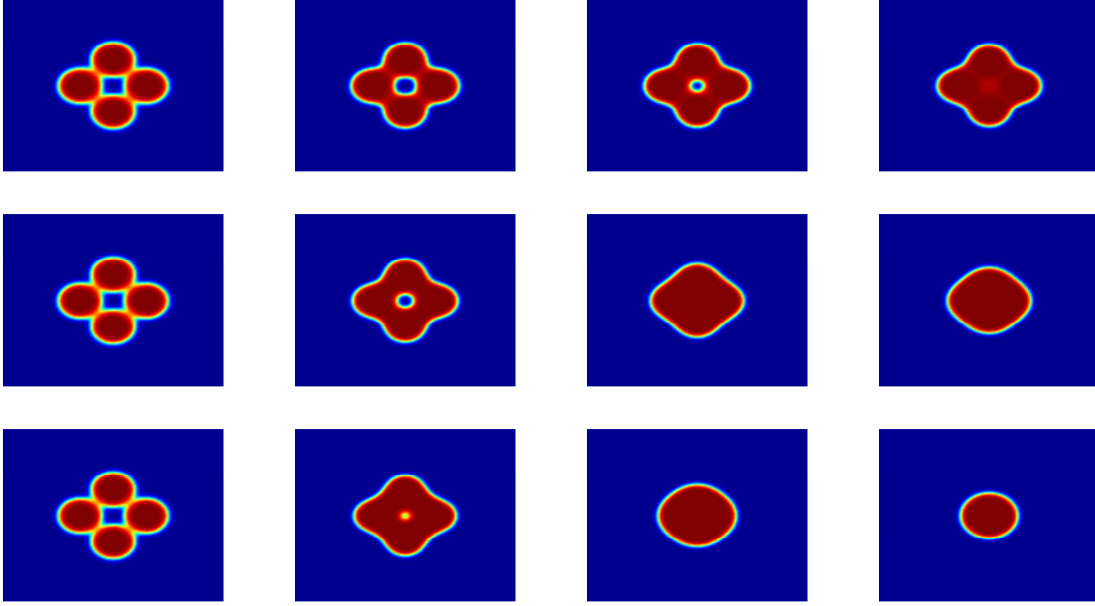


Figure 5: Solution snapshots of Allen-Cahn equation (2.2) at $t = 1, 30, 100, 200$ (from left to right) for three fractional order $\alpha = 0.4, 0.7$ and 0.9 (from top to bottom), respectively.

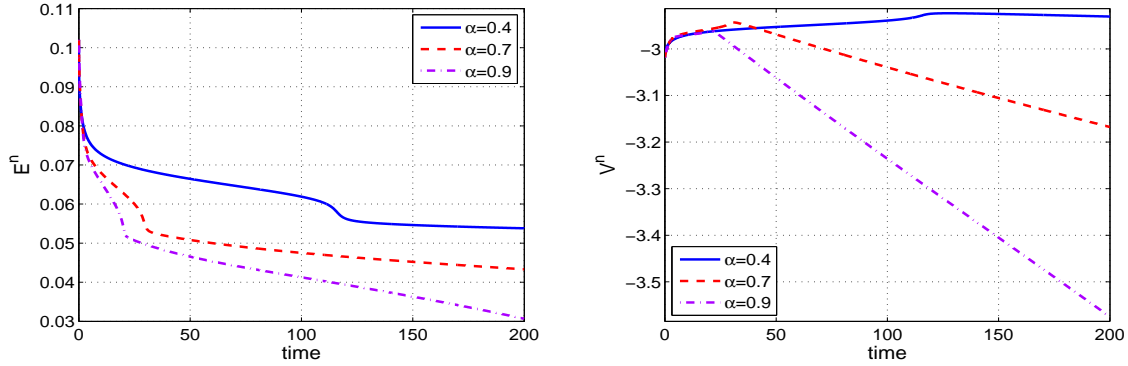


Figure 6: Evolutions of energy and volume curves (from left to right) for the time-fractional Allen-Cahn equation (2.2) with fractional order $\alpha = 0.4, 0.7$ and 0.9 , respectively.

Now we simulate the merging of four drops by the CN-SAV approach with the adaptive time-stepping strategy using the mesh parameters $N_0 = 30$, $T_0 = 0.01$, $\kappa = 10^6$, $\tau_{\min} = \tau_{N_0} = 10^{-3}$ and $\tau_{\max} = 10^{-1}$. The solution snapshots are depicted in Figure 3 and the time evolution of the discrete energy and volume are plotted in Figure 4, respectively. It is apparent that the initial separated four bubbles gradually coalesce into a single big bubble and round up at the end of simulation corresponding to the minimization of the interface area between two phases. The coalescence speed of four bubbles are evidently affected by the fractional index α , that is, the larger the fractional order α is, the faster the coalescence. Also, from Figure 4, we see that the energy decreases in accord with the behavior of numerical solution, and the volume is conserved just as predicted in Theorem 3.3. The solution of time-fractional Allen-Cahn equation (2.2)

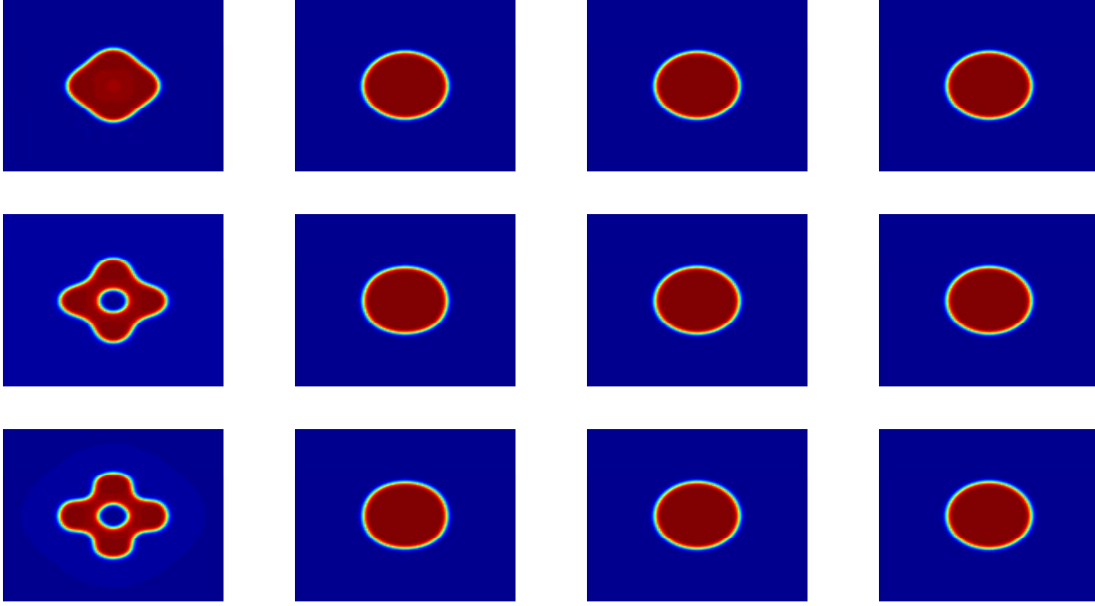


Figure 7: Solution snapshots of the Cahn-Hilliard equation (2.10) at $t = 0.01, 30, 100, 200$ (from left to right) for fractional order $\alpha = 0.4, 0.7$ and 0.9 (from top to bottom), respectively.

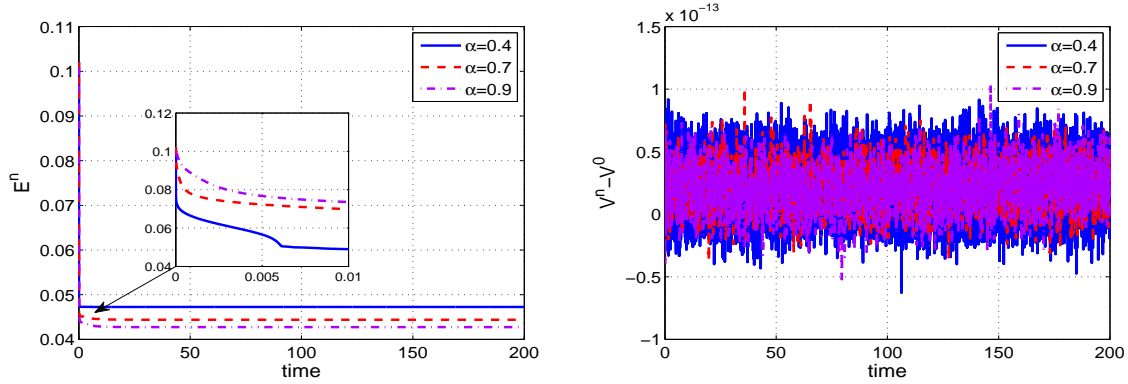


Figure 8: Evolutions of energy and volume curves (from left to right) for time-fractional Cahn-Hilliard equation (2.10) with fractional order $\alpha = 0.4, 0.7$ and 0.9 , respectively.

has a different behavior, see Figures 5-6, the bubble shrinks and finally disappears because the equation (2.2) does not conserve the volume. It is seen that the volume-preserving time-fractional Allen-Cahn equation (2.8) may be a better choice for accurately simulating the coalescence of bubbles than the non-volume-preserving version.

We also use the CN-SAV approach with the *Adaptive Step* approach using $T_0 = 0.01$, $\kappa = 10^3$ and $\tau_{\min} = \tau_{N_0}$ to simulate the time-fractional Cahn-Hilliard equation (2.10). The numerical results are given in Figures 7-8. For three different fractional order $\alpha = 0.4, 0.7, 0.9$, we take $N_0 = 300, 100, 30$, $\gamma = 5, 4, 3$ and $\tau_{\max} = 10^{-2}, 10^{-1}, 10^{-1}$, respectively. Figure 7 shows that the initial bubbles coalesce into one bubble quite rapidly and the steady state is reached immediately. Furthermore, the energy falls off steeply and decays faster for smaller fractional order α , see

Figure 8, so that some extremely small time steps are required to capture this remarkable behavior. Also, it is clear that the volume is conserved during the simulation. Simple comparison from Figures 4 and 8 shows that the energy of time-fractional Cahn-Hilliard equation (2.10) dissipates much faster than that of time-fractional Allen-Cahn equation (2.8) with the nonlocal volume constraint. Correspondingly, the coalescence speed of initial bubbles of the former much faster than that of the latter, see Figures 5 and 7.

4.4 Coarsening dynamics

Example 4.3 We investigate the coarsening dynamics of the conservative time-fractional phase field models with the model parameters $\lambda = 0.1$ and $\varepsilon = 0.05$. If not explicitly specified, we use 128×128 equal distanced meshes in space to discretize the domain $\Omega = (0, 2\pi)^2$. Consider a randomly initial condition by assigning a random number varying from -0.001 to 0.001 at each grid points. Taking the simulating parameters $\beta = 4$ and $C_0 = 1$, we always apply the present CN-SAV methods with the Adaptive Step approach using the following mesh parameters $T_0 = 0.01$, $N_0 = 30$, $\kappa = 10^3$, $\tau_{\min} = \tau_{N_0} = 10^{-3}$ and $\tau_{\max} = 10^{-1}$.

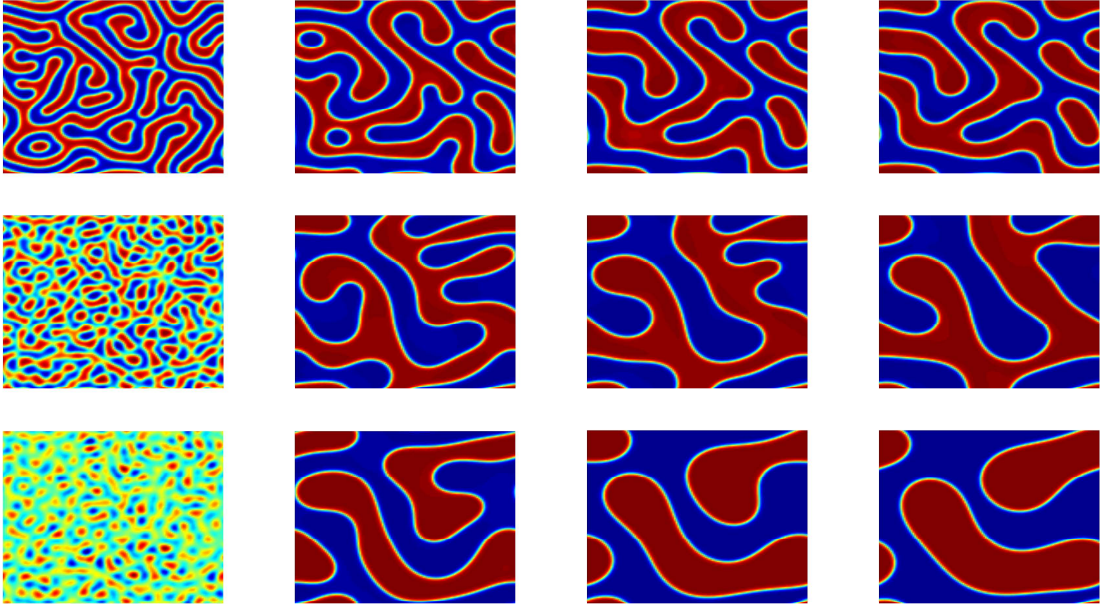


Figure 9: Solution snapshots of coarsening dynamics of (2.10) at $t = 1, 100, 300, 500$ (from left to right) with fractional orders $\alpha = 0.4, 0.7$ and 0.9 (from top to bottom), respectively.

The snapshots of the coarsening dynamics of time-fractional Cahn-Hilliard equation (2.10) with a variety of fractional order α at different time slots are depicted in Figure 9. From the first column of Figure 9, we find that the coarsening dynamics appear to be faster at the early time for smaller fractional order α , while it would be much slower as the time escapes. In other words, the time-fractional Cahn-Hilliard model with larger fractional order α has faster evolution dynamics, which is in good agreement with what we have observed in Example 4.2. In Figure 10, the energy dissipation law scaling $\beta(\alpha)$ is estimated by doing the least square fit

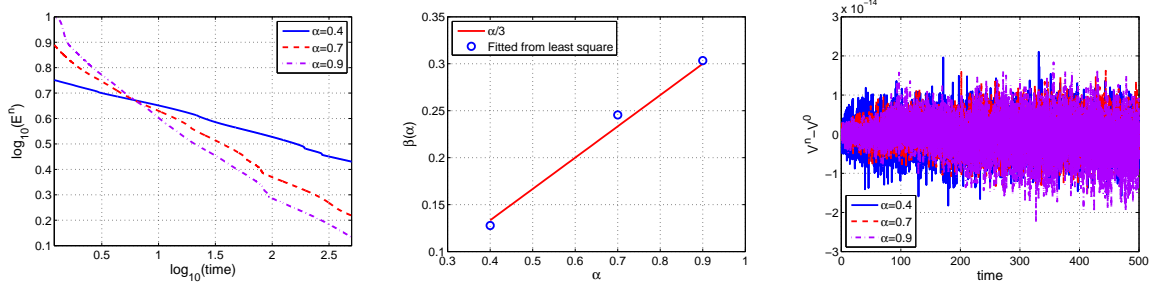


Figure 10: Evolutions of energy, the least square fitted energy dissipation law scaling $\beta(\alpha)$ and volume conservation (from left to right) of the time-fractional Cahn-Hilliard equation for three fractional orders $\alpha = 0.4, 0.7$ and 0.9 , respectively.

via the formula $\log_{10}(E(\alpha, t)) = \beta^0(\alpha) - \beta(\alpha) \log_{10}(t)$. It is observed that the energy dissipates approximately as $O(t^{\frac{\alpha}{3}})$, which is consistent with $O(t^{\frac{1}{3}})$ as $\alpha \rightarrow 1$, as well-known. As expected, the volume is also conserved during the coarsening process.

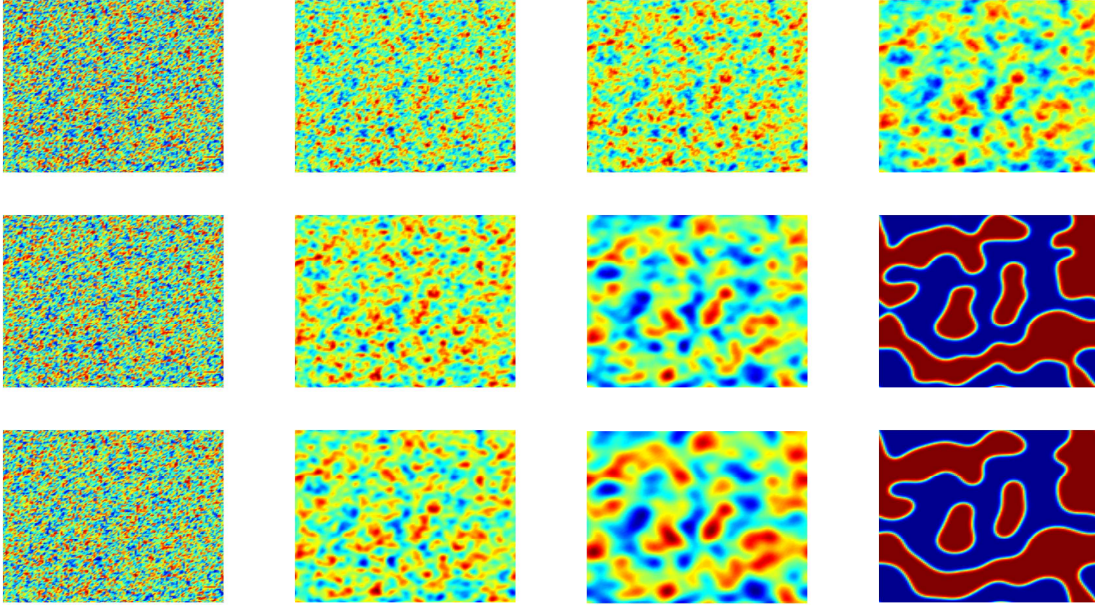


Figure 11: Solution snapshots of coarsening dynamics of the conservative time-fractional Allen-Cahn equation at $t = 1, 100, 300, 500$ (from left to right) for three fractional orders $\alpha = 0.4, 0.7$ and 0.9 (from top to bottom), respectively.

The coarsening snapshots of time-fractional Allen-Cahn equation with volume constraint are depicted in Figure 11. Compared with the numerical results in Figure 9, these phase diagrams generated by the conservative time-fractional Allen-Cahn model have no obvious difference with those produced by the time-fractional Cahn-Hilliard model. Also, from Figure 12, we see that the new model (2.8) preserves the energy dissipation law and the volume well. In summary, the coarsening process of the time-fractional Allen-Cahn (2.8) with volume constraint is slower than that of the time-fractional Cahn-Hilliard model (2.10) because the energy dissipation rate of the

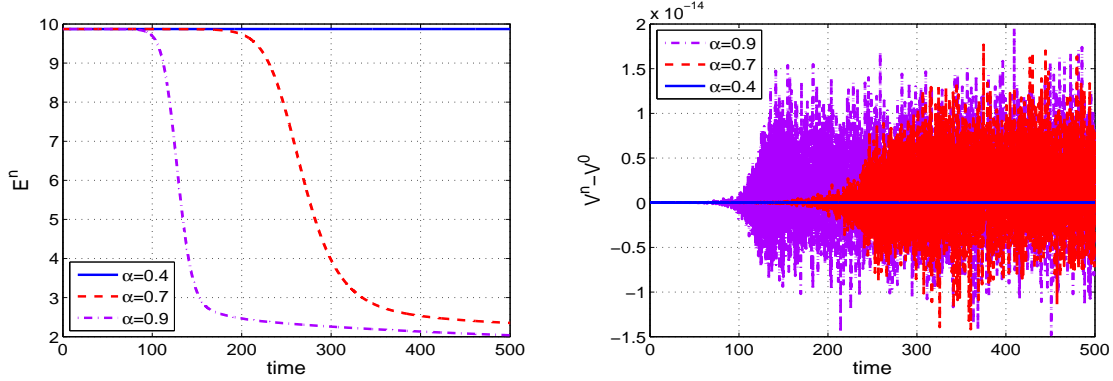


Figure 12: Evolutions of energy and volume (from left to right) of the conservative time-fractional Allen-Cahn equation for fractional orders $\alpha = 0.4, 0.7$ and 0.9 , respectively.

former is smaller; the mechanisms of coarsening dynamics of the two models are quite different although both of them are volume-conserving.

References

- [1] S. Allen and J. Cahn. A microscopic theory for antiphase boundary motion and its application to antiphase domain coarsening. *Acta Metall.*, 27:1085–1095, 1979.
- [2] J. Cahn and J. Hilliard. Free energy of a nonuniform system I. interfacial free energy. *J. Chem. Phys.*, 28:258–267, 1958.
- [3] Y. Gong, J. Zhao, and Q. Wang. Linear second order in time energy stable schemes for hydrodynamic models of binary mixtures based on a spatially pseudospectral approximation. *Adv. Comput. Math.*, 44:1573–1600, 2018.
- [4] C. Krill and L. Chen. Computer simulation of 3-D grain growth using a phase-field model. *Acta Mater.*, 50:3059–3075, 2002.
- [5] Y. Li and J. Kim. Phase-field simulations of crystal growth with adaptive mesh refinement. *Int. J. Heat Mass Transfer*, 55:7926–7932, 2012.
- [6] J. Rubinstein and P. Sternberg. Nonlocal reaction-diffusion equations and nucleation. *IMA J. Appl. Math.*, 48:249–264, 1992.
- [7] M. Brassel and E. Bretin. A modified phase field approximation for mean curvature flow with conservation of the volume. *Math. Methods Appl. Sci.*, 34:1157–1180, 2011.
- [8] T. Hou, T. Tang, and J. Yang. Numerical analysis of fully discretized Crank-Nicolson scheme for fractional-in-space Allen-Cahn equations. *J. Sci. Comput.*, 72:1–18, 2017.
- [9] Z. Li, H. Wang, and D. Yang. A space-time fractional phase-field model with tunable sharpness and decay behavior and its efficient numerical simulation. *J. Comput. Phys.*, 347:20–38, 2017.

- [10] H. Liu, A. Cheng, H. Wang, and J. Zhao. Time-fractional Allen-Cahn and Cahn-Hilliard phase-field models and their numerical investigation. *Comp. Math. Appl.*, 76:1876–1892, 2018.
- [11] H. Lee. High-order and mass conservative methods for the conservative Allen-Cahn equation. *Comput. Math. Appl.*, 72:620–631, 2016.
- [12] D. Lee and J. Kim. Comparison study of the conservative Allen-Cahn and the Cahn-Hilliard equations. *Math. Comput. Simu.*, 119:35–56, 2016.
- [13] J. Shen, C. Wang, X. Wang, and S. Wise. Second-order convex splitting schemes for gradient flows with ehrlich-schwoebel type energy: application to thin film epitaxy. *SIAM J. Numer. Anal.*, 50:105–125, 2012.
- [14] C. Xu and T. Tang. Stability analysis of large time-stepping methods for epitaxial growth models. *SIAM J. Numer. Anal.*, 44:1759–1779, 2006.
- [15] X. Yang, J. Zhao, and Q. Wang. Numerical approximations for the molecular beam epitaxial growth model based on the invariant energy quadratization method. *J. Comput. Phys.*, 333:104–127, 2017.
- [16] J. Shen, J. Xu, and J. Yang. The scalar auxiliary variable (SAV) approach for gradient flows. *J. Comput. Phys.*, 353:407–416, 2018.
- [17] X. Jing, J. Li, X. Zhao, and Q. Wang. Second order linear energy stable schemes for Allen-Cahn equations with nonlocal constraints. *J. Sci. Comput.*, 80:500–537, 2019.
- [18] Y. Gong and J. Zhao. Energy-stable Runge-Kutta schemes for gradient flow models using the energy quadratization approach. *Appl. Math. Lett.*, 94:224–231, 2019.
- [19] T. Tang, H. Yu, and T. Zhou. On energy dissipation theory and numerical stability for time-fractional phase field equations. *arXiv:1808.01471v1*, 2018.
- [20] Q. Du, J. Yang, and Z. Zhou. Time-fractional Allen-Cahn equations: analysis and numerical methods. *arXiv:1906.06584v1*, 2019.
- [21] J. Zhao, L. Chen, and H. Wang. On power law scaling dynamics for time-fractional phase field models during coarsening. *Comm. Non. Sci. Numer. Simu.*, 70:257–270, 2019.
- [22] B. Ji, H.-L. Liao, Y. Gong, and L. Zhang. Adaptive second-order Crank-Nicolson time-stepping schemes for time fractional molecular beam epitaxial growth models. *arXiv:1906.11737v1*, 2019.
- [23] B. Jin, R. Lazarov, and Z. Zhou. An analysis of the L1 scheme for the subdiffusion equation with nonsmooth data. *IMA J. Numer. Anal.*, 36:197–221, 2016.
- [24] B. Jin, B. Li, and Z. Zhou. Numerical analysis of nonlinear subdiffusion equations. *SIAM J. Numer. Anal.*, 56:1–23, 2018.

- [25] H.-L. Liao, D. Li, and J. Zhang. Sharp error estimate of nonuniform L1 formula for time-fractional reaction-subdiffusion equations. *SIAM J. Numer. Anal.*, 56:1112–1133, 2018.
- [26] H.-L. Liao, Y. Yan, and J. Zhang. Unconditional convergence of a fast two-level linearized algorithm for semilinear subdiffusion equations. *J. Sci. Comput.*, 80:1–25, 2019.
- [27] H.-L. Liao, W. Mclean, and J. Zhang. A second-order scheme with nonuniform time steps for a linear reaction-subdiffusion problem. *arXiv:1803.09873v2*, 2018. in review.
- [28] H.-L. Liao, Y. Zhao, and X. Teng. A weighted ADI scheme for subdiffusion equations. *J. Sci. Comput.*, 69:1144–1164, 2016.
- [29] H.-L. Liao, P. Lyu, S. Vong, and Y. Zhao. Stability of fully discrete schemes with interpolation-type fractional formulas for distributed-order subdiffusion equations. *Numer. Algo.*, 75:845–878, 2017.
- [30] Z. Qiao, Z. Zheng, and T. Tang. An adaptive time-stepping strategy for the molecular beam epitaxy models. *SIAM J. Sci. Comput.*, 22:1395–1414, 2011.